AGU PUBLICATIONS

JGR

Journal of Geophysical Research: Space Physics

RESEARCH ARTICLE
10.1002/2015JA021522

Key Points:
- Hot electron enhancements (HEEs) 3–4 times more often on dawnside magnetosheath
- Fluxes of HEEs are twice larger on the dawnside than on the duskside
- The dawn-dusk asymmetry may be caused by processes at quasi-parallel bow shock

Correspondence to:
C.-P. Wang,
cat@atmos.ucla.edu

Citation:
Wang, C.-P., X. Xing, T. K. M. Nakamura, and L. R. Lyons (2015), Dawn-dusk asymmetry in bursty hot electron enhancements in the midtail magnetosheath, *J. Geophys. Res. Space Physics*, *120*, doi:10.1002/2015JA021522.

Received 2 JUN 2015
Accepted 7 AUG 2015
Accepted article online 12 AUG 2015

©2015. American Geophysical Union. All Rights Reserved.

Dawn-dusk asymmetry in bursty hot electron enhancements in the midtail magnetosheath

Chih-Ping Wang[1], Xiaoyan Xing[1], T. K. M. Nakamura[2], and Larry R. Lyons[1]

[1]Department of Atmospheric and Oceanic Sciences, University of California, Los Angeles, California, USA, [2]Space Research Institute, Austrian Academy of Sciences, Graz, Austria

Abstract Bursty (a few minutes) enhancements of hot electrons (1–10 keV) in the tail magnetosheath, which we name hot electron enhancements (HEEs), are sometimes observed. To understand the processes leading to HEEs, we have used 4 years of measurements from Acceleration Reconnection Turbulence and Electrodynamics of Moon's Interaction with the Sun mission to statistically investigate the dawn-dusk asymmetry of HEEs in the midtail (x from -30 to -70 R_E) magnetosheath and their correlations with the solar wind/interplanetary magnetic field (IMF) conditions. We find two strong dawn-dusk asymmetries associated with HEEs: (1) they occur about 3 to 4 times more frequently on the dawnside. (2) Their fluxes on the dawnside are about twice as large as those on the duskside. The magnitudes of HEE fluxes are similar to those of the magnetosphere fluxes near the magnetopause, which are also a factor of 2 higher on the dawnside, indicating that the magnetosphere electrons are likely the source for HEEs and the cause for the HEE flux asymmetry. HEEs occur preferentially during higher solar wind speed, and the majority of HEEs are associated with sharp IMF direction changes and are accompanied by large and transient magnetosheath density changes. These correlations are stronger on the dawnside, suggesting that perturbations created near the quasi-parallel bow shock, which is most of the time on the dawnside, associated with IMF discontinuities is a possible process leading to HEEs and could account for the higher HEE occurrence on the dawnside.

1. Introduction

Recently, using observations from the Acceleration Reconnection Turbulence and Electrodynamics of Moon's Interaction with the Sun (ARTEMIS) mission, we reported that strong and bursty (about a few minutes) enhancements of electron fluxes are sometimes seen in the midtail magnetosheath ($-70 < x < -30$ R_E) at energies from ~1 to 10 keV [*Wang et al.*, 2014] (hereinafter referred to as Paper 1). These energetic electrons have also been observed in more distant magnetosheath ($-70 < x < -100$ R_E) [*Ogasawara et al.*, 2011]. Since 1–10 keV is much higher than the magnetosheath thermal energies, we name these enhancements hot electron enhancements (HEEs). HEEs can be seen at any distances across the magnetosheath from near the magnetopause to near the bow shock. Using simultaneous measurements from the two ARTEMIS probes, in Paper 1 we investigated many HEE events and concluded the following: (1) The hot electrons in HEEs very likely come from the magnetosphere near the current sheet. (2) HEEs are a result of bursty lateral magnetosphere intrusion into the magnetosheath. (3) A single HEE can have a thin and elongated structure as narrow as 2 R_E wide in the x direction, as long as over 7 R_E in the y direction and as thin as 1 R_E in the z direction. (4) HEEs move downtail with speeds similar to the background magnetosheath flows.

The mechanisms and processes that create HEEs remain unclear. In addition to magnetosphere leakage [*Sibeck et al.*, 1987] and magnetopause reconnection [*Scholer et al.*, 1981] that were previously proposed to explain energetic particles observed within the dayside magnetosheath, in Paper 1 we presented an event that indicates that Kelvin-Helmholtz (K-H) perturbations at the magnetopause and subsequent magnetosphere-magnetosheath particle mixing due to either reconnection or diffusion can be a mechanism generating the bursty lateral magnetosphere intrusion and HEEs. Using Geotail observations, previous studies noted a dawn-dusk asymmetry in the enhancements of energetic electrons (> ~38 keV) in the near-Earth magnetosheath [e.g., *Sarafopoulos et al.*, 2000; *Imada et al.*, 2005] but not for low-energy (~3 keV) electrons *Imada et al.*, 2005]. This asymmetry is attributed to higher magnetosphere electron fluxes on the dawnside and leakage of these hot magnetosphere electrons to the magnetosheath. Similarly, the magnetosphere effect may also contribute to dawn-dusk asymmetries observed in different magnetosheath plasma properties [e.g., *Fenner and Freeman*, 1975; *Paularena et al.*, 2001; *Němeček et al.*, 2003]. Therefore, investigating the

dawn-dusk asymmetry of HEEs and their connections with the magnetosphere and with the solar wind/interplanetary magnetic field (IMF) conditions should provide further indications of the processes leading to HEEs.

In this study, we continue from our event study in Paper 1 to statistically analyze HEEs observed by ARTEMIS from August 2010 to October 2014. We describe the ARTEMIS measurements and criteria for selecting HEEs in section 2. In section 3, we present the statistical results, including occurrence, fluxes, correlations with the solar wind/IMF, and their dawn-dusk asymmetries. From these results, we discuss in section 4 the likely processes that can account for the observed dawn-dusk asymmetry in HEE occurrence.

2. Data

The particle and magnetic field measurements from the two ARTEMIS probes (P1 and P2) [*Sibeck et al.*, 2011] are used. The probes orbit the Moon with distances $< \sim 5\ R_E$ from the Moon. ARTEMIS data at lunar distances ($r \sim 60\ R_E$) are available since August 2010. It takes roughly 2 days for each probe to laterally cross the duskside or dawnside magnetosheath. In this study, we investigate the observations from August 2010 to October 2014.

For ions and electrons we use measurements by an electrostatic analyzer (ESA, 0.006–20 keV/q [*McFadden et al.*, 2008]). The magnetic field is measured by the fluxgate magnetometer [*Auster et al.*, 2008]. Onboard plasma moments, omnidirectional energy fluxes, and magnetic field are used, and we interpolated all these parameters having different time resolutions to the same time frame with 1 min resolution. Geocentric solar ecliptic coordinates are used for the probe locations, but the three components of bulk flow and magnetic field are shown in geocentric solar magnetospheric coordinates. One-minute OMNI solar wind and IMF parameters that have been shifted to the Earth's bow shock nose were used. An additional simple time shift from the x locations of the bow shock nose to the ARTEMIS location estimated using the solar wind speed $|V_x|$ was then added.

We selected HEE with the following procedures: (1) We first selected magnetosheath data on the nightside using criteria: $x < 0$ and $|y| \leq 60\ R_E$, electron temperature (T_e) ≤ 70 eV, energy flux for 9 keV electrons $\leq 2 \cdot 10^4$ eV/s sr cm^2 eV, and the bulk speed (V_x) and density (N) satisfy either ($V_x \leq -200$ km/s and $N \geq 2$ cm^{-3}) or ($V_x \leq -300$ km/s and $N \geq 0.9$ cm^{-3}). (Note that the criteria are based on the experience from examining all magnetopause crossings. The criteria cannot exclude solar wind plasma, but most of these solar wind data points are removed later by the procedure described in the next paragraph.) (2) From these magnetosheath data, we computed hourly median values of the energy fluxes for 1, 4, and 9 keV electrons, and these values are used as the background fluxes. (3) A data point was selected as an enhancement if its 1 keV electron flux is a factor of 3 larger and its 4 and 9 keV fluxes are larger than the background fluxes. Note that we have tried different factors for the enhancements. Using a higher factor gives a lower number of HEEs, but it does not affect the conclusions presented in this study, especially for the dawn-dusk asymmetries. Figures 1a and 1b show examples of ARTEMIS crossing the duskside and dawnside magnetosheath and magnetopause, respectively. As indicated by the white arrows in the electron energy spectra for a few examples of HEEs, HEEs can be identified as the spikes of enhanced electron fluxes above ~1 keV (see Figure 3 of Paper 1 for the energy spectra of individual HEEs). It can be seen that HEEs were observed throughout the magnetosheath at different y distances away from the magnetopause on both dawnside and duskside.

For the magnetosheath and HEE data points selected from the above procedure, we further estimate how far they are from the magnetopause and from the bow shock. The probes usually encounter the boundaries multiple times because of the boundary's lateral motion due to either changes in the solar wind/IMF conditions or due to magnetopause processes. Thus, for each ARTEMIS pass across the duskside or dawnside tail, we first chose the main bow shock and magnetopause locations from the multiple boundary crossings. For example, as shown in Figure 1b, there are many magnetopause crossings from ~03:00 to 15:00 UT. However, it is clear that the crossing of the main magnetopause should be at ~08:00 UT as indicated by the vertical dotted line, since the crossings seen afterward are a result of sporadic appearance of the magnetosphere/low-latitude boundary layer (LLBL). Following this approach, we visually inspected each ARTEMIS pass within a long time scale (24 h) and chose the main magnetopause crossing as the one outside which the appearance of magnetosphere/LLBL is only sporadic. Similarly, we chose the main bow shock location for each pass. Figures 2a and 2b show the

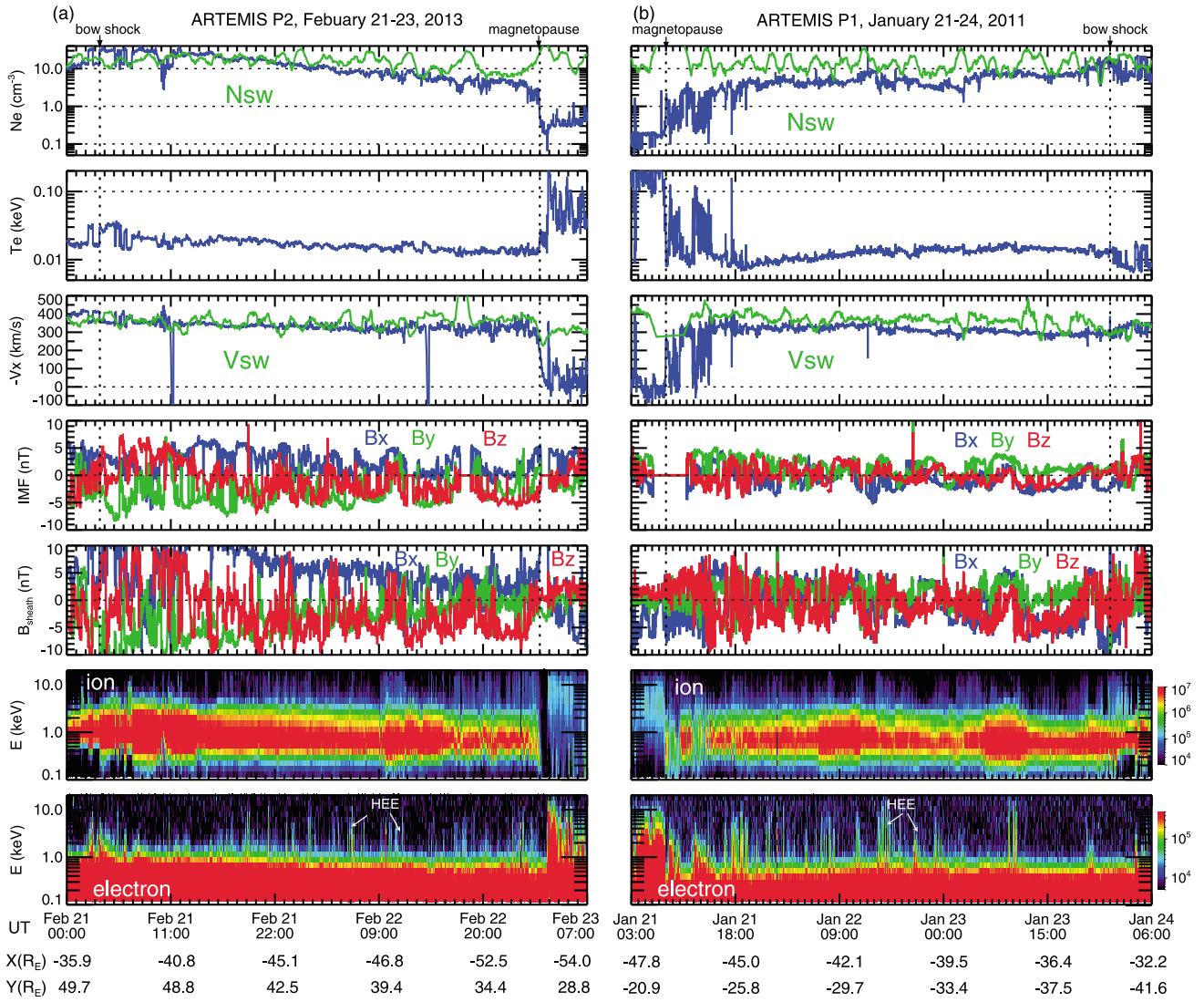

Figure 1. From top to bottom: electron density (solar wind density in green), electron temperature, $-V_x$ (solar wind speed in green), IMF components, B components, and omnidirectional ion and electron fluxes (eV/(s sr cm^2 eV)) observed by (a) ARTEMIS P2 on 21–23 February 2013 and by (b) P1 on 21–23 January 2011. The vertical dotted lines indicate the magnetopause and bow shock.

locations of the main magnetopause (purple crosses) and bow shock (black squares) on the duskside and dawnside, respectively. So for each pass, we can estimate the y distances of each magnetosheath or HEE data point to the main magnetopause and bow shock locations. We use the main magnetopause and bow shock locations to further exclude unwanted or ambiguous data points for this statistical study by only using the magnetosheath and HEE data points that satisfy two conditions: (1) outside the main magnetopause and $|dy| \leq 20\ R_E$, where $dy = y_{\mathrm{probe}} - y_{\mathrm{magnetopause}}$, since the typical magnetosheath width at this tail distance is about 20 R_E, and (2) inside the main bow shock and at least 2 R_E away from the bow shock. The condition (2) allows us to exclude most of the solar wind data inside the main bow shock that cannot be excluded earlier by the magnetosheath data criteria. Note that the data points within sporadic magnetosphere/LLBL intervals outside the main magnetopause, despite satisfying condition (1), have already been excluded earlier by our magnetosheath data criteria. The locations of these selected HEEs are shown in Figures 2a and 2b as the red dots. There are 2746 HEEs on the dawnside and 967 on the duskside. Figures 2c and 2d show the probability distributions for the duration of HEEs (in red) and time separation between two consecutive HEEs (in blue). The duration for the majority of HEEs is less than ~2 min while they are separated from each other by a few minutes. There are no distinguishable differences in both the durations and separations between the duskside and dawnside HEEs.

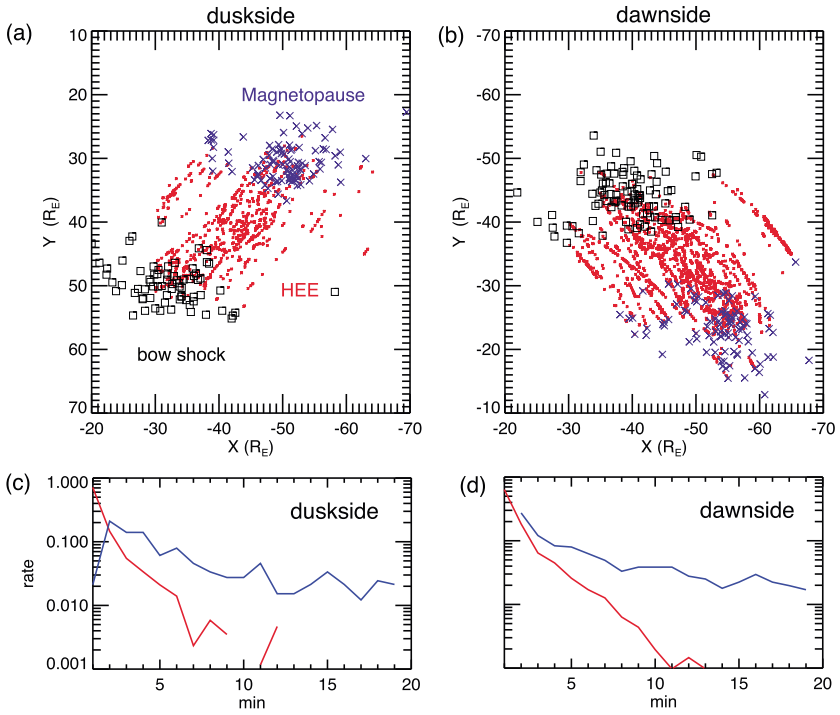

Figure 2. The *x-y* locations of HEEs (red dots), the main magnetopause (purple crosses), and the main bow shock (black squares) on (a) the duskside and (b) dawnside. Probability distributions of the duration of HEEs (red) and the separations between two consecutive HEEs (blue) on (c) the duskside and (d) dawnside.

3. Results

3.1. HEE Occurrence

Figure 3a shows the number of the 1 min data points for magnetosheath data (purple) and for HEEs (red) as a function of *y* on the top and the ratios of the number of HEEs to that of magnetosheath (occurrence rates) on the bottom (note that the magnetosheath data points also include the HEE data points). Figures 3b shows the same numbers and ratios as Figure 3a but as a function of *dy* with the positive (negative) *dy* for the duskside (dawnside). The number of magnetosheath data points is relatively the same at different *dy* and has no clear dawn-dusk asymmetry. On the other hand, there is a strong dawn-dusk asymmetry for HEEs with the occurrence rates a factor of 3 to 4 higher on the dawnside than on the duskside. On the dawnside, the occurrence rates are slightly higher closer to the magnetopause, while no clear *dy* dependence is seen on the duskside. We will discuss in section 4 the likely processes leading to the higher HEE occurrence rates on the dawnside. In the previous studies for energetic electrons in the near-Earth magnetosheath mentioned in the Introduction, occurrence rates were not specifically investigated.

3.2. HEE Fluxes

Figure 4a shows the energy fluxes for HEE 4 and 9 keV electrons as a function of *dy*. It can be seen that the fluxes are substantially higher on the dawnside than the duskside. Figure 4b shows the statistical comparisons of the HEE electron energy spectra (median values with the vertical lines indicating with 25% and 75% quartiles) between the dawnside (in red) and duskside (in blue) near the magnetopause ($|dy| \leq 5\ R_E$). The dawnside HEE fluxes from ~1 to 10 keV are clearly higher by a factor up to ~2. Figure 4c shows that in the magnetosheath the dawnside fluxes are only slightly higher than the duskside fluxes. Thus, the roughly dawn-dusk symmetric magnetosheath electron fluxes are likely not the cause for the higher dawnside HEE fluxes. Rather, the slightly higher dawnside magnetosheath fluxes are likely due to the inclusion of the higher dawnside HEE fluxes.

In Paper 1, we concluded that HEEs are likely magnetospheric electrons escaping to the magnetosheath. We thus compare the magnetosphere electron energy spectra between the dawnside and duskside magnetosphere near the magnetopause ($|dy| \leq 5\ R_E$ on the magnetosphere side). The magnetosphere data are chosen

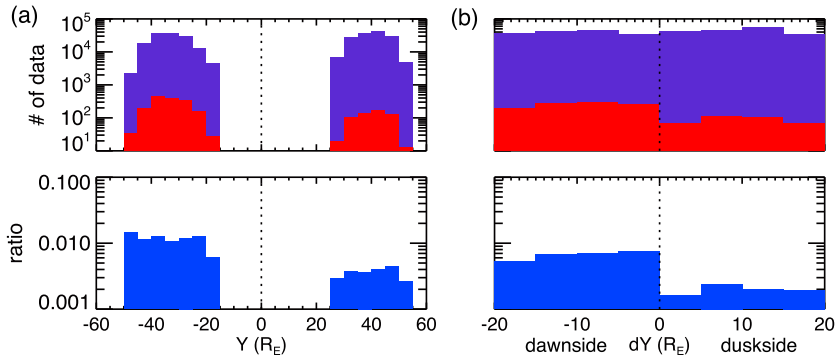

Figure 3. (top) Number of 1 min data points for the magnetosheath (purple) and HEEs (red) and (bottom) the ratios of the number of HEEs to that of the magnetosheath data as a function of (a) *y* and (b) *dy*. Positive (negative) *dy* indicates the duskside (dawnside).

with the criteria: $N \leq 0.8\,\mathrm{cm}^{-3}$, $|V| \leq 100$ km/s, and $|B| \leq 10$ nT. The comparisons, as shown in Figure 4d, clearly show that the dawnside magnetosphere electron fluxes are higher than the duskside fluxes within the energy range of ~0.5 to 10 keV. The dawnside fluxes are higher by a factor of ~2, similar to that seen in the HEE flux dawn-dusk asymmetry. Figures 4e and 4f show that the HEE fluxes (in red) are substantially higher than the magnetosheath fluxes (in black) and are within the range of magnetosphere fluxes at energies $>$ ~2 keV on both the duskside and dawnside. These comparisons further support our previous conclusion that the magnetosphere electrons are the source for HEEs. That the HEE fluxes are similar to the magnetosphere fluxes only at $>$ ~2 keV should be associated with the magnetopause processes creating HEEs. How this develops may be answered by future theoretical or simulation studies. However, the observed connection attributes the dawn-dusk asymmetry in HEE fluxes to the dawn-dusk asymmetry in the magnetosphere electrons. In the previous studies that show higher fluxes of energetic electrons observed on the dawnside of the near-Earth magnetosheath [e.g., *Imada et al.*, 2005], the magnetosphere electrons as a source was also used to explain the dawn-dusk asymmetry. We compared the solar wind/IMF conditions for our selected magnetosphere data between the dawnside and duskside (not shown here) and ruled out the possibility that the dawn-dusk asymmetry seen in magnetosphere fluxes is due to a bias in their corresponding upstream conditions. This dawn-dusk asymmetry in the magnetosphere keV electrons in the midtail region may possibly result from electron's dawnward magnetic drift, but it is beyond the scope of this study to determine whether magnetic drift or other magnetospheric processes are responsible.

Despite the dawn-dusk asymmetry in the magnetosphere electron fluxes being able to explain the dawn-dusk asymmetry in the HEE fluxes, this is less likely to account for the dawn-dusk asymmetry in the HEE occurrence. As shown in Figures 4e and 4f, even though the magnetosphere fluxes are lower on the duskside, they are still significantly higher than the duskside magnetosheath fluxes. Thus, the asymmetry in the HEE occurrence is more likely related to the processes causing HEEs.

3.3. Correlations With Solar Wind and IMF

To understand the occurrence of HEEs, we investigated whether they occur preferentially under certain solar wind/IMF conditions. Figures 5a and 5b show two dawnside magnetosheath passes by P1 on 16 and 17 August 2011 (event 1) and 22 and 23 December 2010 (event 2), respectively. As compared with event 2, event 1 had lower density, higher flow speed, and more fluctuated magnetic field directions in both the solar wind and magnetosheath, and many more HEEs. In both events, most of these HEEs occurred near the time when there was a sharp change in the B_z direction.

To investigate statistically the preferred solar wind/IMF conditions suggested above, we plot in Figures 6a and 6c the probability distributions for the plasma and magnetic field parameters in the magnetosheath corresponding to HEEs (in red) in comparison with those to all magnetosheath data (in blue) on the dawnside and duskside, respectively. We also use Bootstrap method to estimate the uncertainty of these probability distributions. We first obtained 1000 data sets that are random resampled from the original data set for either HEE or magnetosheath data. We then computed the 95% confidence intervals (mean ± 1.96·standard

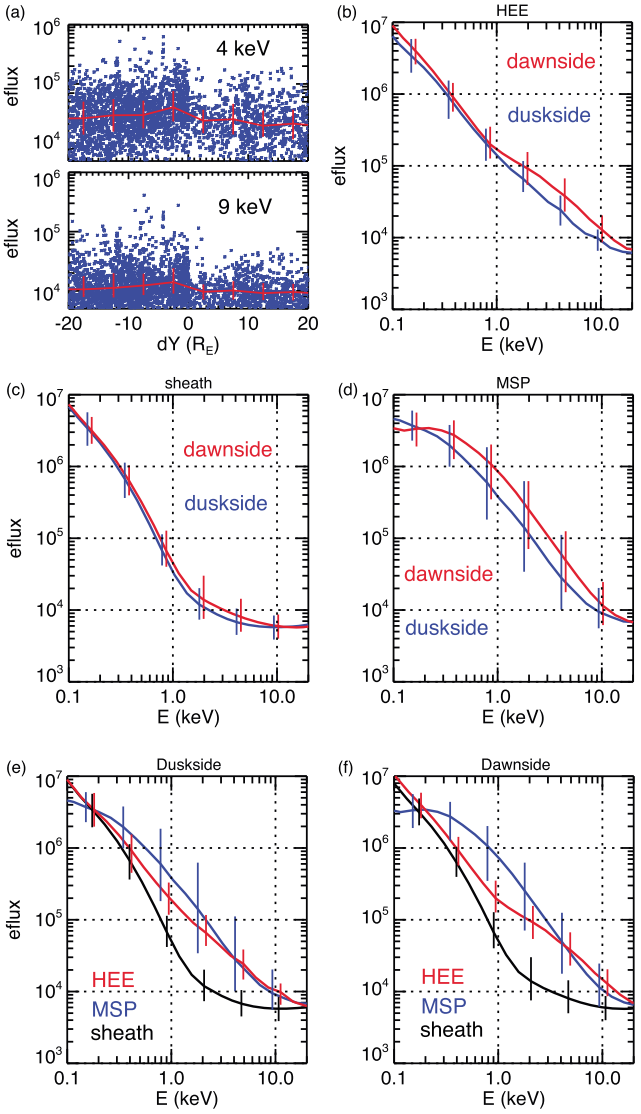

Figure 4. (a) Omnidirectional fluxes (eV/(s sr cm^2 eV)) for (top) 4 keV and (bottom) 9 keV electrons in HEEs. Comparisons of the energy spectra between the dawnside (red) and duskside (blue) near the magnetopause ($|dy| \leq 5\ R_E$) for (b) HEEs, (c) magnetosheath, and (d) magnetosphere electrons (the curves are the median values and the vertical lines indicate the 25% and 75% quartiles). Comparisons of the HEE energy spectra (red) with the magnetosheath (black) and magnetosphere (blue) on (e) duskside and (f) dawnside.

deviation) from the 1000 data sets. The confidence intervals are indicated by the dotted lines in Figure 6. Here we use the magnetosheath plasma and magnetic field to represent the solar wind/IMF conditions since they reflect more precisely in time the concurrent solar wind/IMF conditions than do the OMNI solar wind/IMF data. This is important to our investigation since a HEE only lasts for ~2 min but the uncertainty in OMNI solar wind/IMF is much larger due to the estimated time shift first from the solar wind monitors to the bow shock nose and then to the ARTEMIS locations. For references, Figures 6b and 6d show the same investigations but using OMNI solar wind/IMF data. Compared with typical magnetosheath, it is clear that on the dawnside HEEs occur during periods of relatively lower solar wind/magnetosheath density, and thus higher solar wind/magnetosheath speed (since the solar wind density and speed is well anticorrelated), statistically confirming the correlations indicated by the two events shown in Figure 5. However, this correlation with higher solar wind speed is much weaker on the duskside. Furthermore, HEEs occur more often when the magnitude of IMF/magnetosheath B_z is smaller. To check the possible connection between HEEs and the B_z direction changes suggested in Figure 5, we define a parameter, dB_z, to indicate sharpness of the B_z changes within a 10 min period ($t \pm 5$ min) corresponding to a data point at time t, $dB_z = (|B_{z,\,max}| - |B_{z,\,min}|)/[\text{sign}(B_{z,\,max}) \cdot \text{sign}(B_{z,\,min})]$, where $B_{z,\,max}$ ($B_{z,\,min}$) and sign($B_{z,\,max}$) (sign($B_{z,\,min}$)) are the magnitude and sign of the maximum (the minimum) B_z (either IMF B_z or the magnetosheath B_z). So if B_z change within the 10 min is shaper, then $|dB_z|$ is larger, and dB_z is negative if there is a B_z direction change. It can be seen that HEEs are more often associated with negative dB_z with 75% (66%) for HEEs on the dawnside (duskside) compared with 39% (37%) for the magnetosheath data. The high percentages indicate that the correlations between HEEs and negative dB_z are not due to coincidence. Thus, the smaller B_z magnitudes for HEEs are due to B_z becoming smaller as it changes direction near the time of HEEs.

Because of draping of magnetic field lines within the magnetosheath, the magnetosheath B_{xy} angle (defined as 0° at noon and increases eastward) is more similar to the IMF B_{xy} angle on the side of the magnetosheath where the bow shock is quasi-perpendicular (the IMF direction is perpendicular to the bow shock normal) but is rotated by about 90° on the other side of the magnetosheath where the bow shock is quasi-parallel. As shown in Figure 6, for all magnetosheath data (in blue), the probability distributions for the B_{xy} angles peak

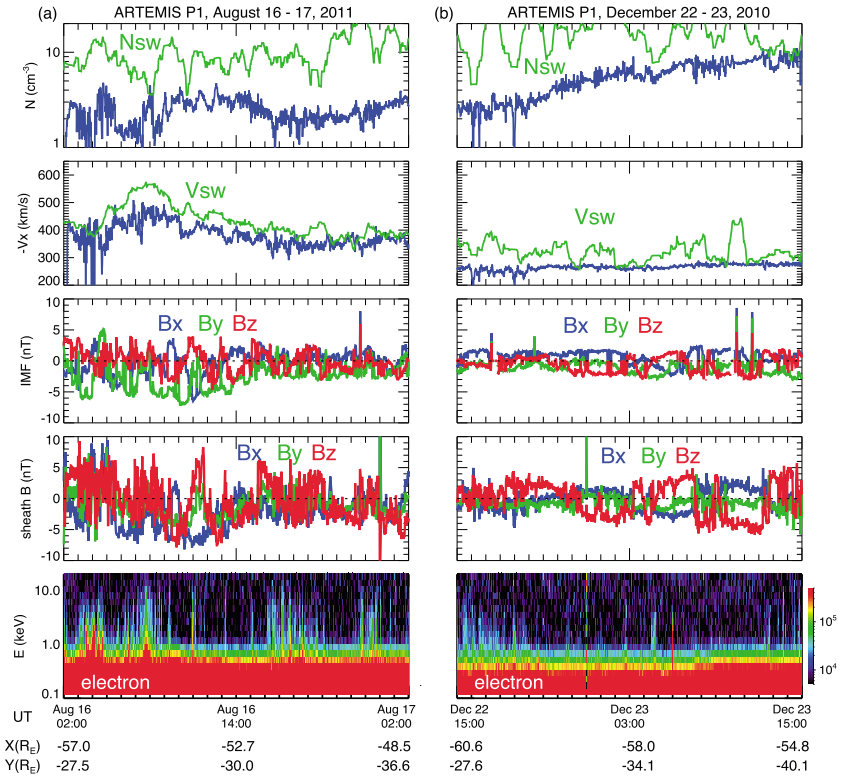

Figure 5. From top to bottom: electron density (solar wind density in green), $-V_x$ (solar wind speed in green), IMF components, B components, and omnidirectional electron fluxes (eV/(s sr cm^2 eV)) observed by P1 on (a) 16–17 August 2011 and (b) 22–23 December 2010.

at ~45° and 225° on the dawnside and peak at and ~135° and 315° on the duskside, indicating that the corresponding IMF is a Parker spiral (~135° or 315°) most of the time. For HEEs (in red) on the dawnside, the probabilities of their B_{xy} angles at ~45° and 225° become higher than those for all magnetosheath data, indicating that the dawnside HEEs occur preferentially when the quasi-parallel bow shock is on the dawnside. On the other hand, the probabilities of the B_{xy} angles for the duskside HEEs at ~45° and 225° are significantly lower than those of all magnetosheath data, indicating more than coincidence that some, but not the majority, of the duskside HEEs occur under an anti-Parker spiral IMF (~45° or 225°), that is, when the quasi-parallel bow shock is on the duskside. These suggest that there may be a connection between the processes at the quasi-parallel bow shock and HEEs. Possible processes leading to this connection are further discussed in section 4.2. The above correlations with solar wind plasma and magnetic fields are much less clearly seen when using OMNI data, and we attribute this to the large uncertainty due to the time shifting.

The above preferred solar wind and IMF conditions for HEEs are more clearly seen on the dawnside than on the duskside, suggesting a possible connection between the upstream solar wind/IMF conditions and the higher HEE occurrence rates on the dawnside. We further discuss in section 4 the likely processes that lead to this connection.

4. Discussion

As indicated in Paper 1, HEEs are a result of transient magnetosphere intrusion into the magnetosheath and the associated secondary processes, such as reconnection and diffusion. The dawn-dusk asymmetry in HEE occurrence is thus likely a result of a dawn-dusk asymmetry in the processes that cause the transient magnetosphere intrusion. In this section we investigate and discuss whether K-H perturbations and bow shock processes can provide the connection between HEEs and their preferred solar wind/IMF conditions shown in section 3.3 and can account for the dawn-dusk asymmetry in HEE occurrence presented in section 3.1.

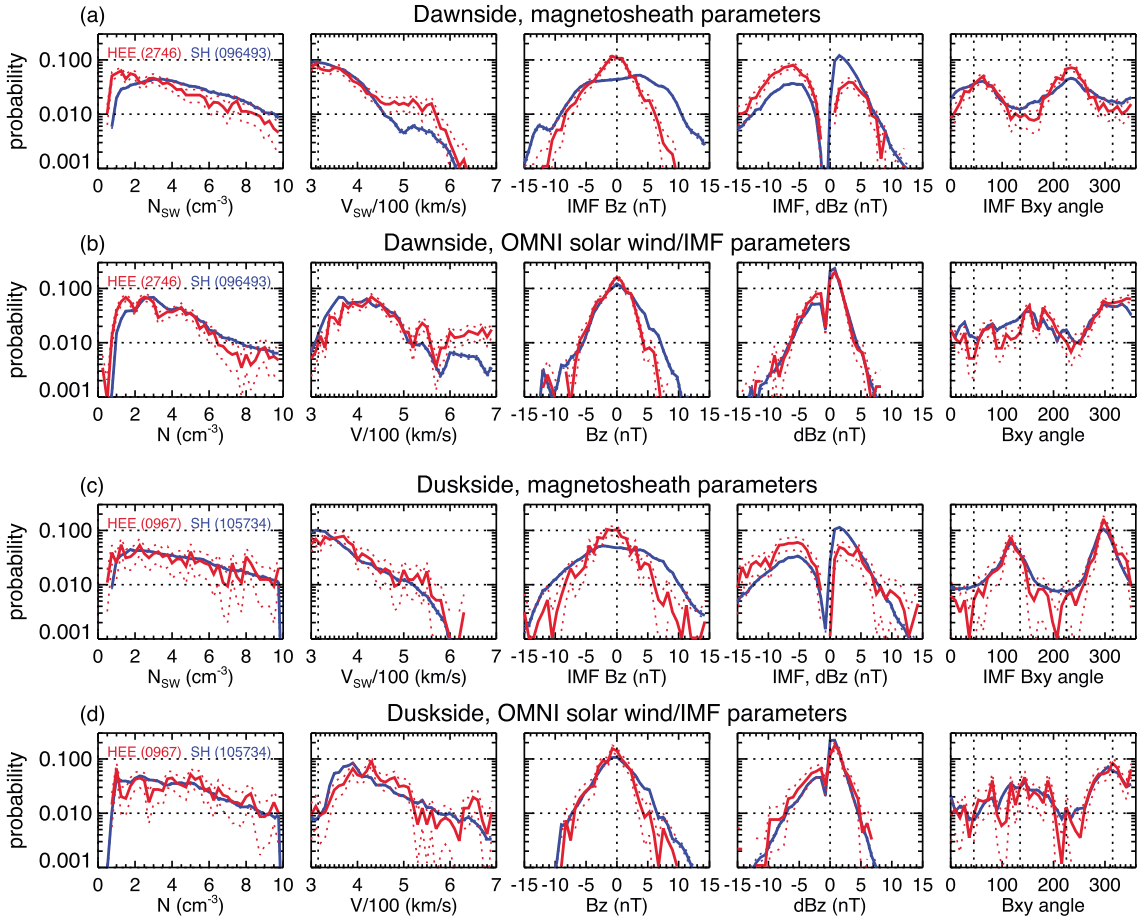

Figure 6. Probability distributions of density, flow speed, B_z, dB_z, and B_{xy} angle (see text for definitions of dB_z and B_{xy} angle) observed by ARTEMIS for the magnetosheath (blue) and HEEs data (red) on (a) the dawnside and (c) duskside. Probability distributions of the solar wind density, solar wind flow speed, IMF B_z, B_z/B_{xy} (IMF), dB_z (IMF), and IMF B_{xy} angle from OMNI (including additional time shift from the bow shock nose to ARTEMIS locations) corresponding to the magnetosheath (blue) and HEEs data (red) on (b) the dawnside and (d) duskside. The numbers inside the parenthesis indicate the number of data points for each data set. The dashed lines above and below the solid lines indicate the 95% confidence intervals (see text).

4.1. Kelvin-Helmholtz Perturbations

That the HEEs occur more often during periods when IMF B_z direction is more fluctuating, as shown in Figure 5, and during higher solar wind speed, as shown in Figure 6, suggests a likely connection of HEEs with Alfvénic solar wind. Within Alfvénic solar wind, which is believed to be a result of Alfvén waves in the solar corona mixed with convective structure [*Tu and Marsch*, 1995], there are larger fluctuations in the IMF directions and solar wind density/speed than normal solar wind. The solar wind is more likely to be Alfvénic when the solar wind speed is higher. By including Alfvénic fluctuations in IMF directions and solar wind speeds in global MHD simulations, *McGregor et al.* [2014] showed that enhanced flow shear at the magnetopause associated with the Alfvénic fluctuations enhances K-H waves along the flanks. As suggested in Paper 1 that K-H waves and associated secondary processes, such as reconnection and diffusion, can be one of the possible mechanisms for HEEs, the MHD simulation results thus provide an explanation for the connection between HEEs and Alfvénic solar wind. In the *McGregor et al*. simulations there is no clear dawn-dusk asymmetry in the occurrence of K-H waves, likely due to the assumption of IMF $B_x = 0$. *Nykyri* [2013] considered Parker spiral IMF in global MHD simulations and found that the K-H growth rate is larger on the dawnside than on the duskside. However, it is also not conclusive from observations whether there is a dawn-dusk asymmetry in K-H perturbations, since contradicting conclusions have be drawn from different observational studies of K-H waves in the near-Earth flanks [e.g., *Hasegawa et al.*, 2006; *Taylor et al.*, 2012; *Lin et al.*, 2014]. Additionally, how these K-H perturbations evolve as they propagate to the midtail flanks remains unknown.

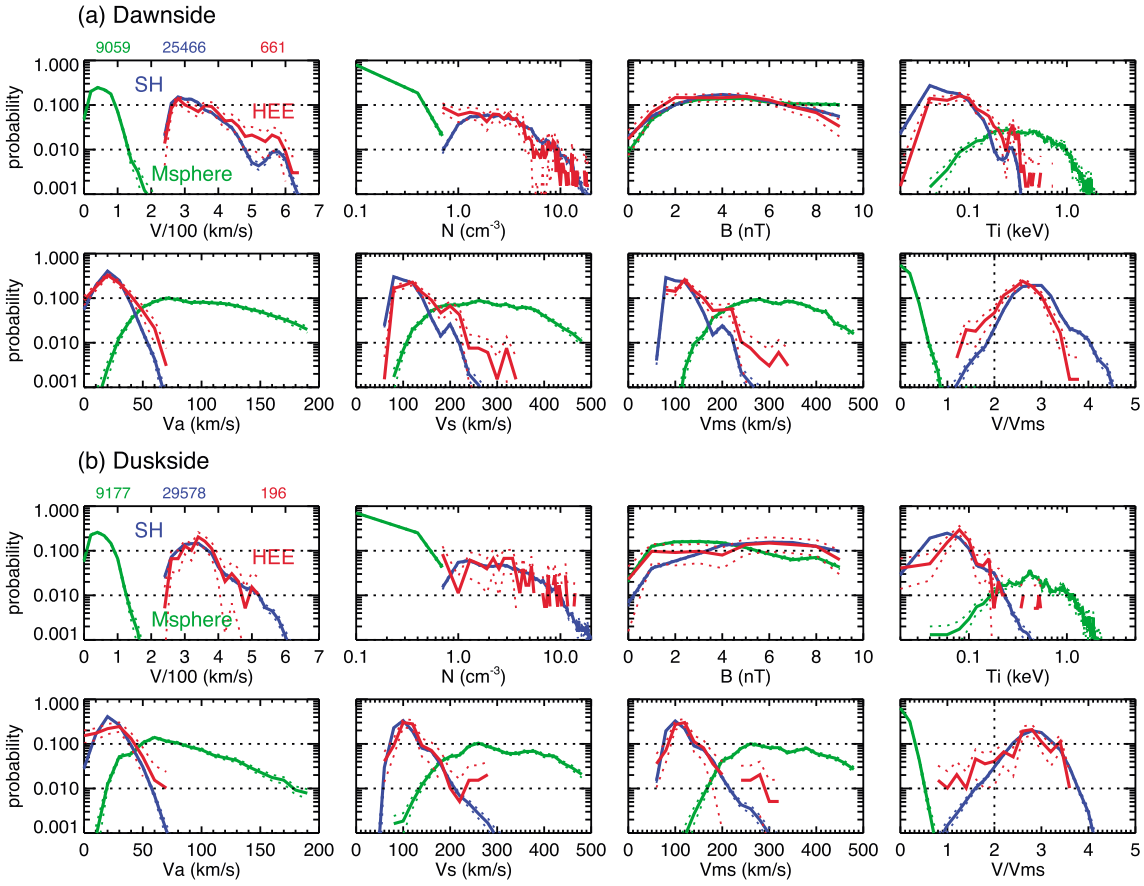

Figure 7. Flow speed, density, magnetic field strength, ion temperature, Alfvén speed (V_a), sound speed (V_s), magnetosonic speed (V_{ms}), magnetosonic Mach number (V/V_{ms}) for HEEs (red), magnetosheath (blue), and magnetosphere (purple) on (a) the dawnside and (b) duskside. The numbers on the top indicate the number of data points for each data set. The dashed lines above and below the solid lines indicate the 95% confidence intervals.

Therefore, considering HEEs caused by the K-H perturbations propagating from the near-Earth flanks, our current understanding is not sufficient to indicate whether they can account for the dawn-dusk asymmetry in HEE occurrence.

The nightside domain of *McGregor et al.*'s simulations only extends to $x = -25\ R_E$ so it is not known whether the K-H waves can still occur locally in the midtail. Considering compressible plasma and finite boundary thickness, *Miura and Pritchett* [1982] and *Miura* [1992] showed that the K-H instability is determined by the magnetosonic speeds (V_{ms}, ${V_{ms}}^2 = {V_a}^2 + {V_s}^2$, where V_a is the Alfvén speed and V_s is the sound speed) on both the magnetosphere and magnetosheath sides relative to a perturbation. Simulations showed that if the flow speeds relative to a tailward propagating perturbation on both sides are slower than the magnetosonic speed, that is the magnetosonic Mach number $M_{ms} = V/V_{ms} < 1$, the perturbation can be locally K-H unstable [*Kobayashi et al.*, 2008]. As the magnetosheath flow speed increases with increasing downtail distances, the condition may become less favorable for unstable K-H. Therefore, we examined statistically the conditions on either sides of the midtail magnetopause ($|dy| \leq 3\ R_E$). Figure 7 shows that most of the time M_{ms} across the magnetopause is much higher than 2; thus, the flow shear condition for a perturbation propagating at any speed is not favorable for unstable K-H. In comparison, for HEEs the temperature distribution shifts to higher values while the M_{ms} distribution shifts to lower values so that the probability for $M_{ms} < 2$ becomes higher. Since, as shown in Figure 6, the solar wind speed is higher for HEEs compared with typical magnetosheath and statistically the magnetosheath ion temperature is higher when the solar wind speed is higher [*Wang et al.*, 2012], this suggests that during higher solar wind speed the midtail magnetopause can become more K-H unstable and lead to more HEEs. However, Figure 7 shows that only a small number of the HEE events occur under the favorable K-H unstable conditions and the number is higher on the duskside (~7% on the

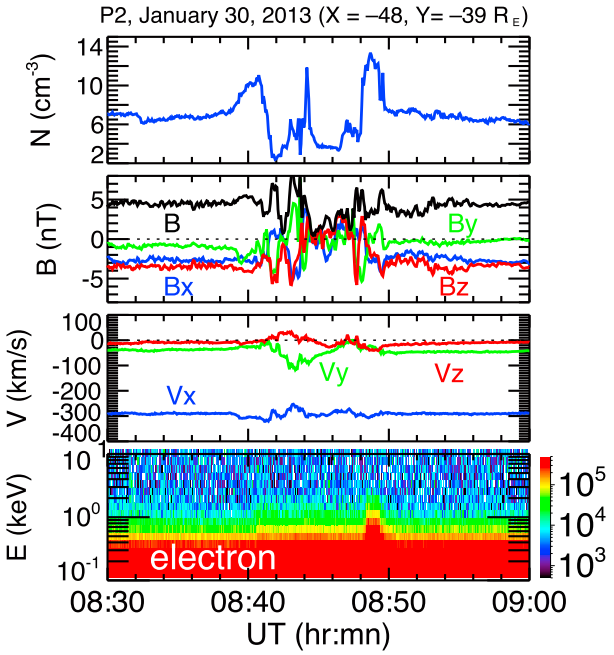

Figure 8. A HFA-like event. From top to bottom: density, *B* components, flow velocity components, and omnidirectional electron fluxes (eV/(s sr cm^2 eV)) observed by P2 on 30 January 2013.

dawnside and ~13% on the duskside). Therefore, even though the K-H perturbations can be one of the mechanisms for HEEs, there is no strong indication that it would result in higher HEE occurrence rates on the dawnside.

4.2. The Bow Shock Perturbations

There are some transient perturbations at the bow shock that occur preferentially when there is a sharp IMF direction change associated with an IMF discontinuity, such as hot flow anomalies (HFAs) [e.g., *Thomsen et al.*, 1986; *Schwartz*, 1995; *Zhang et al.*, 2010] and foreshock bubbles (FBs) [e.g., *Omidi et al.*, 2010; *Turner et al.*, 2013]. These perturbations are believed to be created by kinetic interaction between IMF discontinuities and the bow shock or foreshock, so that our current physical understanding is mainly from hybrid simulations. It has been shown that HFAs and FBs can create transient density fluctuations (a time scale of a few minutes and a spatial scale of a few to 10 R_E) and thus variations in the dynamic pressure in the magnetosheath, resulting in localized deformation of the dayside magnetopause. Using three THEMIS probes, two near the magnetopause and one near the bow shock, *Archer et al.* [2015] showed an event of a transient (~1 min) outward motion of the dayside magnetosphere into the magnetosheath observed by the two probes near the magnetopause, which is a result of a FB observed by the probe just upstream of the bow shock. Therefore, as a transient HFA or FB perturbation moves downstream to the midtail magnetosheath, it may continue to cause magnetosphere intrusion into the magnetosheath, which can explain the bursty and localized magnetosphere intrusion associated with HEEs shown in Paper 1. In addition, Figure 6 of Paper 1 shows three examples of HEEs moving downstream with the same speeds as the background magnetosheath flows, which is consistent with the expectation if they are associated with a tailward moving HFA or FB.

Figure 8 shows a transient perturbation observed by P2 on the dawnside magnetosheath at $x \sim -50\ R_E$ with well-defined characteristics of a HFA typically seen on the dayside. With the perturbation, B_z changed sharply from ~ −4 nT to ~3 nT then back to −4 nT from 08:40 to 08:50 UT. The same B_z change was seen by Cluster ~20 min earlier in the upstream solar wind at x~12 and y~10 R_E and $V_x \sim -340$ km/s. For the perturbation seen by P2, there is a low density and magnetic field core at ~08:45 UT sandwiched by two walls of high density and magnetic field at ~08:40 and 08:49 UT, respectively. The flow direction within the perturbations is substantially diverted. This perturbation is found to be accompanied by a weak HEE seen at ~08:49 UT. This example indicates that the density perturbations associated with HFAs or FBs can be a likely mechanism for creating magnetosphere intrusion and HEEs. In our survey, HEEs are often associated with transient and substantial density changes that are not due to changes in the upstream solar wind density. To investigate the association with transient density changes, we define a parameter, dN/N, as $(N_{max} - N_{min})/N_{ave}$, where N_{max}, N_{min}, and N_{ave} are the maximum, minimum, and average values of densities within the ±5 min period of a data point. Figure 9 shows that the transient density changes associated with HEEs are substantially larger compared to the typical magnetosheath data. This association is more clearly seen on the dawnside, similar to the associations with the solar wind speeds and transient B_z changes shown in Figure 6.

It has been found that HFAs [*Šafránková et al.*, 2000] and FBs [*Turner et al.*, 2013] occur more often when the solar wind speed is higher. Therefore, it is plausible that during Alfvénic solar wind, the IMF directions change

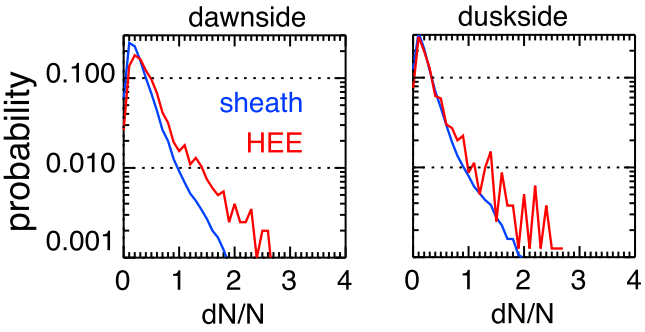

Figure 9. Probability distributions for *dN/N* (see text for definition) for HEEs (red) and magnetosheath (blue) on the (left) dawnside and (right) duskside.

more frequently and the more IMF discontinuities can create more HFAs and FBs and thus likely lead to more HEEs. Since HFAs and FBs are generated in the quasi-parallel bow shock, which is on the dawnside most of the time due to the Parker spiral IMF, the connection of HEEs with HFAs and FBs may explain the higher occurrence rates on the dawnside. This may also explain the correlations between the dawnside HEEs with the Parker spiral IMF and the correlation between the duskside HEEs and anti-Parker spiral IMF shown in Figure 6. In addition to HFAs and FBs, there are other types of density or dynamic pressure perturbations created in association with the quasi-parallel bow shock, such as spontaneous HFAs [*Zhang et al.*, 2013], magnetosheath filamentary structures [*Omidi et al.*, 2014], transient flux enhancements or jets [e.g., *Němeček et al.*, 1998; *Hietala et al.*, 2012], or large-scale low-frequency electromagnetic wavefronts [*Karimabadi et al.*, 2014]. But these perturbations can occur without IMF discontinuities. If they also create HEEs, they will also contribute to the dawn-dusk HEE occurrence asymmetry, but their resulting HEEs will not be associated with a change in the magnetic field direction. However, our current understanding of these bow shock perturbations is limited to the dayside region. It remains mostly unknown as to how they evolve as they drift tailward to the midtail and whether these perturbations can be created in the midtail bow shock. Therefore, future studies investigating these bow shock perturbations in the midtail and their effects on the magnetosphere will help us further understand HEEs and transient solar wind-magnetosphere coupling.

5. Summary

Using 4 years of ARTEMIS measurements, we have statistically investigated the dawn-dusk asymmetries of HEEs in the midtail magnetosheath and their correlations with the solar wind/IMF conditions. HEEs can be observed at any *y* distances from the magnetopause. Our key findings are the following:

1. There is dawn-dusk asymmetry in HEE occurrence rates with the rates about a factor of 3 to 4 higher on the dawnside.
2. There is a dawn-dusk asymmetry in HEE fluxes from ~1 to 10 keV. The HEE fluxes at 4 keV on the dawnside are as twice large as on the duskside. The HEE fluxes are significantly larger than the background magnetosheath fluxes and are within the range of magnetosphere fluxes. There is also a dawn-dusk asymmetry in the magnetosphere electrons, with the fluxes in 1–10 keV also about a factor of 2 higher on the dawnside. This indicates strongly that magnetosphere electrons are likely the source for HEEs and the cause for the dawn-dusk asymmetry in HEE fluxes.
3. Compared with typical magnetosheath data, HEEs occur during higher solar wind speed. The majority of HEEs are associated with sharp transient IMF direction changes and are accompanied by large transient magnetosheath density changes. These correlations are stronger on the dawnside. The correlation with IMF B_{xy} angles suggests a connection of HEEs with the quasi-parallel bow shock.
4. Higher solar wind speed can result in flow shear conditions at the midtail magnetopause more favorable for unstable K-H. However, only a smaller number of HEEs occur when the flow shear conditions are locally K-H unstable and the number is larger on the duskside. Also, it is not conclusive from observations whether the near-Earth K-H perturbations have a dawn-dusk asymmetry. So K-H perturbations are likely not the main mechanism causing the higher dawnside HEE occurrence.
5. The correlations with higher solar wind speed, sharp IMF direction changes, IMF B_{xy} angles, and transient and large magnetosheath density changes described in (3) suggest a connection of HEEs with perturbations created near the quasi-parallel shock associated with IMF discontinuities, such as HFAs and FBs. Since the quasi-parallel shock is most often on the dawnside, this connection is likely to account for the higher HEE occurrence rates on the dawnside.

Acknowledgments
We thank Hui Zhang at University of Alaska, Drew Turner at Aerospace Corporation, and Vassilis Angelopoulos at University of California, Los Angeles, for their helpful discussion. The work by C.-P. Wang and L.R. Lyons has been supported by NASA grant NNX11AJ12G and NSF grant ATM-1003595. The work by X. Xing has been supported by NASA grant NNX12AD11G. We acknowledge NASA contract NAS5-02099 for ARTEMIS; C.W. Carlson and J.P. McFadden for the use of ESA data; and K.H. Glassmeier, U. Auster, and W. Baumjohann for the use of FGM data provided under DLR contract 50 OC 0302. The ARTEMIS data are available online (http://artemis.ssl.berkeley.edu/) for free. We thank J.H. King, N. Papatashvilli at AdnetSystems, NASA GSFC, and CDAWeb for providing the OMNI data.

Yuming Wang thanks the reviewers for their assistance in evaluating this paper.

References

Archer, M. O., D. L. Tuner, J. P. Eastwood, S. J. Schwartz, and T. S. Horbury (2015), Global impacts of a foreshock bubble: Magnetosheath, magnetopause, and ground-based observations, *Planet. Space Sci.*, *106*, doi:10.1016/j.pss.2014.11.026.

Auster, H. U., et al. (2008), The THEMIS fluxgate magnetometer, *Space Sci. Rev.*, *141*, 235–264, doi:10.1007/s11214-008-9365-9.

Fenner, M. A., and J. W. Freeman Jr. (1975), Dawn-dusk magnetosheath plasma asymmetries at 60 R_E, *J. Geophys. Res.*, *80*(25), 3693–3697, doi:10.1029/JA080i025p03693.

Hasegawa, H., M. Fujimoto, K. Takagi, Y. Saito, T. Mukai, and H. Reme (2006), Single-spacecraft detection of rolled-up Kelvin-Helmholtz vortices at the flank magnetopause, *J. Geophys. Res.*, *111*, A09203, doi:10.1029/2006JA011728.

Hietala, H., N. Partamies, T. V. Laitinen, L. B. N. Clausen, G. Facskó, A. Vaivads, H. E. J. Koskinen, I. Dandouras, H. Rème, and E. A. Lucek (2012), Supermagnetosonic subsolar magnetosheath jets and their effects: From the solar wind to the ionospheric convection, *Ann. Geophys.*, *30*, 33–48, doi:10.5194/angeo-30-33-2012.

Imada, S., M. Hoshino, and T. Mukai (2005), The dawn-dusk asymmetry in magnetosheath and the leakage of energetic electrons: The Geotail observation, in *Frontiers in Magnetospheric Plasma Physics: Celebrating 10 Years of Geotail Operation*, *Cospar Colloq. Ser.*, vol. 16, edited by M. Hoshino et al., pp. 34–39, Elsevier, New York.

Karimabadi, H., et al. (2014), The link between shocks, turbulence, and magnetic reconnection in collisionless plasmas, *Phys. Plasmas*, *21*, 062308, doi:10.1063/1.4882875.

Kobayashi, Y., M. Kato, K. T. A. Nakamura, T. K. M. Nakamura, and M. Fujimoto (2008), The structure of Kelvin–Helmholtz vortices with super-sonic flow, *Adv. Space Res.*, *41*(8), 1325–1330.

Lin, D., C. Wang, W. Li, B. Tang, X. Guo, and Z. Peng (2014), Properties of Kelvin-Helmholtz waves at the magnetopause under northward interplanetary magnetic field: Statistical study, *J. Geophys. Res. Space Physics*, *119*, 7485–7494, doi:10.1002/2014JA020379.

McFadden, J. P., C. W. Carlson, D. Larson, V. Angelopoulos, M. Ludlam, R. Abiad, B. Elliott, P. Turin, and M. Marckwordt (2008), The THEMIS ESA plasma instrument and in-flight calibration, *Space Sci. Rev.*, *141*, 277–302, doi:10.1007/s11214-008-9440-2.

McGregor, S. L., M. K. Hudson, and W. J. Hughes (2014), Modeling magnetospheric response to synthetic Alfvénic fluctuations in the solar wind: ULF wave fields in the magnetosphere, *J. Geophys. Res. Space Physics*, *119*, 8801–8812, doi:10.1002/2014JA020000.

Miura, A. (1992), Kelvin-Helmholtz instability at the magnetospheric boundary: Dependence on the magnetosheath sonic Mach number, *J. Geophys. Res.*, *97*(A7), 10,655–10,675, doi:10.1029/92JA00791.

Miura, A., and P. L. Pritchett (1982), Nonlocal stability analysis of the MHD Kelvin-Helmholtz instability in a compressible plasma, *J. Geophys. Res.*, *87*(A9), 7431–7444, doi:10.1029/JA087iA09p07431.

Němeček, Z., J. Šafránková, L. Prech, D. G. Sibeck, S. Kokubun, and T. Mukai (1998), Transient flux enhancements in the magnetosheath, *Geophys.Res. Lett.*, *25*(8), 1273–1276, doi:10.1029/98GL50873.

Němeček, Z., M. Hayosh, J. Šafránková, G. N. Zastenker, and J. D. Richardson (2003), The dawn-dusk asymmetry of the magnetosheath: INTERBALL-1 observations, *Adv. Space Res.*, *31*(5), 1333–1340.

Nykyri, K. (2013), Impact of MHD shock physics on magnetosheath asymmetry and Kelvin-Helmholtz instability, *J. Geophys. Res. Space Physics*, *118*, 5068–5081, doi:10.1002/jgra.50499.

Ogasawara, K., S. A. Livi, D. G. Mitchell, T. P. Armstrong, and N. Krupp (2011), Properties of energetic particle bursts at dawnside magnetosheath: Cassini observations during the 1999 Earth swing-by, *J. Geophys. Res.*, *116*, A12207, doi:10.1029/2011JA016813.

Omidi, N., J. P. Eastwood, and D. G. Sibeck (2010), Foreshock bubbles and their global magnetospheric impacts, *J. Geophys. Res.*, *115*, A06204, doi:10.1029/2009JA014828.

Omidi, N., D. Sibeck, O. Gutynska, and K. J. Trattner (2014), Magnetosheath filamentary structures formed by ion acceleration at the quasi-parallel bow shock, *J. Geophys. Res. Space Physics*, *119*, 2593–2604, doi:10.1002/2013JA019587.

Paularena, K. I., J. D. Richardson, M. A. Kolpak, C. R. Jackson, and G. L. Siscoe (2001), A dawn-dusk density asymmetry in Earth's magnetosheath, *J. Geophys. Res.*, *106*(A11), 25,377–25,394, doi:10.1029/2000JA000177.

Šafránková, J., L. Přech, Z. Němeček, D. G. Sibeck, and T. Mukai (2000), Magnetosheath response to the interplanetary magnetic field tangential discontinuity, *J. Geophys. Res.*, *105*(A11), 25,113–25,121, doi:10.1029/1999JA000435.

Sarafopoulos, D. V., M. A. Athanasiu, D. G. Sibeck, R. W. McEntire, E. T. Sarris, and S. Kokubun (2000), Energetic proton and electron dispersion signatures in the nightside magnetosheath support their leakage out of the magnetopause, *J. Geophys. Res.*, *105*(A7), 15,729–15,740, doi:10.1029/2000JA900041.

Scholer, M., F. M. Ipavich, G. Gloeckler, D. Hovestadt, and B. Klecker (1981), Leakage of magnetospheric ions into the magnetosheath along reconnected field lines at the dayside magnetopause, *J. Geophys. Res.*, *86*(A3), 1299–1304, doi:10.1029/JA086iA03p01299.

Schwartz, S. J. (1995), Hot flow anomalies near the Earth's bow shock, *Adv. Space Res.*, *15*, 107–116, doi:10.1016/0273-1177(95)00025-A.

Sibeck, D. G., R. W. McEntire, A. T. Y. Lui, R. E. Lopez, S. M. Krimigis, R. B. Decker, L. J. Zanetti, and T. A. Potemra (1987), Energetic magnetospheric ions at the magnetopause: Leakage or merging?, *J. Geophys. Res.*, *92*(A11), 12,097–12,114, doi:10.1029/JA092iA11p12097.

Sibeck, D. G., et al. (2011), ARTEMIS science objectives, *Space Sci. Rev.*, *165*, 59–91, doi:10.1007/s11214-011-9777-9.

Taylor, M. G. G. T., et al. (2012), Spatial distribution of rolled-up Kelvin-Helmholtz vortices at Earth's dayside and flank magnetopause, *Ann. Geophys.*, *30*, 1025–1035, doi:10.5194/angeo-30-1025-2012.

Thomsen, M. F., J. T. Gosling, S. A. Fuselier, S. J. Bame, and C. T. Russell (1986), Hot, diamagnetic cavities upstream from the Earth's bow shock, *J. Geophys. Res.*, *91*(A3), 2961–2973, doi:10.1029/JA091iA03p02961.

Tu, C.-Y., and E. Marsch (1995), MHD structures, waves and turbulence in the solar wind: Observations and theories, *Space Sci. Rev.*, *73*, 1–210.

Turner, D. L., N. Omidi, D. G. Sibeck, and V. Angelopoulos (2013), First observations of foreshock bubbles upstream of Earth's bow shock: Characteristics and comparisons to HFAs, *J. Geophys. Res. Space Physics*, *118*, 1552–1570, doi:10.1002/jgra.50198.

Wang, C.-P., M. Gkioulidou, L. R. Lyons, and V. Angelopoulos (2012), Spatial distributions of the ion to electron temperature ratio in the magnetosheath and plasma sheet, *J. Geophys. Res.*, *117*, A08215, doi:10.1029/2012JA017658.

Wang, C.-P., X. Xing, T. K. M. Nakamura, L. R. Lyons, and V. Angelopoulos (2014), Source and structure of bursty hot electron enhancements in the tail magnetosheath: Simultaneous two-probe observation by ARTEMIS, *J. Geophys. Res. Space Physics*, *119*, 9900–9918, doi:10.1002/2014JA020603.

Zhang, H., D. G. Sibeck, Q.-G. Zong, S. P. Gary, J. P. McFadden, D. Larson, K.-H. Glassmeier, and V. Angelopoulos (2010), Time History of Events and Macroscale Interactions during Substorms observations of a series of hot flow anomaly events, *J. Geophys. Res.*, *115*, A12235, doi:10.1029/2009JA015180.

Zhang, H., D. Sibeck, Q. G. Zong, N. Omidi, D. Turner, and L. N. Clausen (2013), Spontaneous hot flow anomalies at quasi-parallel shocks: 1. Observations, *J. Geophys. Res. Space Physics*, *118*, 1–7, doi:10.1002/jgra.50376.